Unit-Area Analysis of Friction Stir Welding Data

Kevin Colligan

Concurrent Technologies Corporation
Johnstown, PA, USA

Synopsis

The present study developed analytical techniques for analysis of welds from various thickness and welding tool designs by expressing the variables of interest in terms of unit area of welding tool surface. Previously, a method of expressing the spindle torque on a unit-area basis resulted in a calculation of the average flow stress in the workpiece at the tool/workpiece interface. This approach was extended here to the calculation of average heat flux and average energy density, which express aspects of welding tool geometry, workpiece thickness, travel speed, spindle speed and observed spindle torque. Additionally, the forge force and resultant in-plane lateral forces on the welding tool are analyzed in terms of tool surface area to yield shoulder pressure and lateral probe pressure. These unit-area quantities are analyzed in this ongoing study with reference to machine settings, excess flash production, macro-section characteristics, defect formation and tensile strength in FSW of aluminum alloys. In welding experiments conducted in 1-in and 2-in 7075 aluminum plate, it was observed that the flow stress response surface with respect to volumetric flowrate and the inverse of the surface velocity forms a plane for each thickness of workpiece, implying that the flow stress response surface is possibly planar for other thermal boundary conditions. This was confirmed by analysis of the FSW Data Set published earlier. It was also found that in a series of welds made with decreasing flow stress, below a threshold of about 24 MPa, weld defects were produced. This same threshold was observed in 25mm and 50mm 7075-T6 welds, implying that this threshold may be universal for a given alloy. To test the practical utility of this observation, welds were made in 25mm 7075 in plates with variable width while using manual changes to travel speed and spindle speed to maintain a constant value of flow stress in the weld. The results suggest that a welding controller that manipulates spindle speed and travel speed to produce a constant flow stress that is well above the identified threshold can produce defect-free welds despite changing boundary conditions, such as changing joint geometry.

Introduction

Friction stir welding procedures are defined by several basic variables which describe the welding tool and workpiece geometry, the machine settings and a number of other details. Often, these parameters become part of the welding procedure specification that is qualified for production of a particular product. However, a greater understanding of the welding procedure can be gained by using the most basic variables to calculate more meaningful data features to represent aspects of the process. As a simple analogy, it is more meaningful to describe a container by its volume rather than by its more basic features of diameter and length.

The author previously published a friction stir welding data set [1,2], comprising a diverse collection of welding procedures collected from published and unpublished sources. Although spindle speed, travel speed and spindle torque are known to have key roles in the generation and dissipation of heat, it is difficult to draw useful conclusions regarding welding procedures in general from these basic variables. The goal of unit-area analysis is to provide a means of normalizing FSW data to produce new data features that are more

meaningful, with implications for welding specifications, machine control, quality assessment and other topics of interest in the field.

Another motivation for this work stemmed from the growing application of machine learning in manufacturing technologies. To train an algorithm that is useful for general-purpose friction stir welding, utilizing data that represents the underlying physical processes is essential. To this end, the unit-area analysis described here was developed to normalize the data from welding procedures with different tool and workpiece geometries. Normalizing data is a key aspect of data pre-processing for algorithm training, and it is hypothesized that models will achieve higher performance when trained on the engineered features opposed to raw sensor outputs. Other derived quantities, not necessarily based on the area of the welding tool surface, are also meaningful with respect to machine learning.

Significant work has been done to relate the basic variables in FSW to more meaningful derived quantities, most notably with respect to heat generation and dissipation. Researchers have developed various approaches to expressing heat generation in FSW, often as input to models for predicting temperature distribution during welding. The earliest approaches represented the heat as coming from the shoulder only, assuming a circular heat source on the plate surface to calculate heat input from an assumed friction coefficient or based on the workpiece shear flow stress, acting on the shoulder area [4-9]. Analysis of the contact conditions between the tool and matrix followed [10-17], leading to the conclusion that heat generation could be best represented as being based on the shear flow stress acting on all tool surfaces in contact with the workpiece. In 2002, an important analytical step was made by relating the spindle torque to the shear flow stress of the matrix, assuming a uniform average shear flow stress distributed over the tool surfaces [13, 14]. A detailed analysis was developed by Schmidt, et al., [15] which concluded that in FSW, the contact conditions in FSW of aluminum generate plastic deformation over most of the tool surfaces, except for a small region at the periphery of the shoulder, where frictional heating generates very close to the same heat as the sticking condition. Based on these analyses, it was concluded that the spindle torque can be represented as the summation of an average contact shear stress distributed over the tool/workpiece interface. This is presented here in terms of an average normal stress in the workpiece, described previously [2, 3].

In this work, unit-area analysis was examined with respect to its implications for machine control. Various methods of closed-loop control of friction stir welds have been demonstrated. Methods have broadly been based on force and temperature [18-26]. Force-based methods, employed since the very beginning of FSW research, focused primarily on the axial force component as a means of controlling welding tool depth to maintain constant welding conditions with variable workpiece alignment relative to the elevation of the welding head, or to compensate for welding machines that have variable stiffness over the envelope, such as for robotic systems or for systems with a very large envelope. Temperature-based control has been shown to be very successful in maintaining constant welding conditions in the face of variable weld boundary conditions by using thermocouples embedded in the rotating welding tool to measure the tool temperature very near the tool/workpiece interface. Torque control demonstrated by Longhurst, et al [27, 28] was employed with the goal of ensuring constant shoulder engagement with the workpiece surface, in contrast to the method described here.

Unit-Area Analysis

Unit-area analysis seeks to combine welding tool geometry, machine settings and measured forces to form derived quantities that are more meaningful to characterization of welding conditions than the constituent basic variables. The important variables in this formulation

are summarized in Table 1. Note that some of the derived quantities are not strictly "per unit area" but are nonetheless useful aspects of the analysis.

Table 1. Summary of derived quantities.

Process Inputs	
G Parameter (average), mm^3	Average (radius x area) of tool surface
Surface Velocity (average), m/s	Area-based average tool surface velocity
Volumetric Flowrate, mm^3/s	Volume of workpiece material swept by the tool profile per unit time
Process Outputs	
Flow Stress (average), MPa	Resistance to tool rotation per unit tool area
Shoulder Pressure, MPa	Axial pressure based on shoulder outer diameter
Lateral Probe Pressure, MPa	In-plane force resultant divided by probe profile area
Heat Flux, W/mm^2	Power output per unit tool area
Energy Density, J/mm^3	Energy input per unit volume of material swept by the tool

Parameter G

Parameter G [29], previously referred to as "geo" [2, 3], refers to a mathematical summation of the incremental areas of the tool surface multiplied by their radii. The term is useful in unit-area analysis for the calculation of flow stress and surface velocity, and it captures the essential welding tool geometry for this use. G is defined as:

$$G = \int_S r \, dA \tag{1}$$

The solutions for (1) depend on the form of the welding tool. For a concave or flat shoulder, a frustrum or cylindrical probe and a flat probe tip,

$$G = \frac{2\pi}{3}\left[\frac{S^3 - {P_r}^3}{\cos\alpha} + \frac{t\left((P_R+P_T)^2 - P_R P_T\right)}{\cos\beta} + {P_T}^3\right], \text{ (units: length}^3\text{)} \tag{2}$$

where,

$\alpha = shoulder\ taper\ angle$
$\beta = frustum\ probe\ half\ angle$
$S = shoulder\ radius$
$P_R = probe\ root\ radius$
$P_T = probe\ tip\ radius$
$t = workpiece\ thickness, or\ probe\ length$

Complete equations for flat, tapered and convex shoulders and frustum or cylindrical probes are given in the Data Set Topic document, available for download with the FSW Data Set [1].

Surface Velocity

An area-based surface velocity was derived previously [2, 3]. In the past, researchers have attempted to normalize spindle speed to account for differences in tool size by simply expressing the maximum surface velocity at the periphery of the shoulder or at the surface of

a cylindrical probe. The present approach mathematically sums the surface velocity of each incremental area of the tool as,

$$\text{Average surface velocity} = \omega\bar{r} = \frac{\omega \int_S r\, dA}{total\ surface\ area} \tag{3}$$

The surface integral in the numerator is equal to G, from equations (1) and (2), resulting in,

$$\omega\bar{r} = \omega \left[\frac{\frac{2}{3}\left[\frac{S^3 - {P_R}^3}{\cos\alpha} + \frac{t\left((P_R+P_T)^2 - P_R P_T\right)}{\cos\beta} + {P_T}^3\right]}{\frac{(S+P_R)(S-P_R)}{\cos\alpha} + \frac{t(P_R+P_T)}{\cos\beta} + {P_T}^2} \right], \text{(units: length per unit time)} \tag{4}$$

Again, complete equations for various tool styles are given in the Data Set Topics document.

Volumetric Flowrate

Volumetric flowrate (FR) is simply a measure of the volume of material swept by the welding tool per unit time and is calculated as the travel speed multiplied by the profile area of the probe, with units of cubic length per unit time. The calculation of weld pitch was an early attempt at normalizing the travel speed, expressed as the travel speed divided by the spindle speed [30]. However, this form confounded travel speed with spindle speed and did not account for differences in workpiece thickness. Another version of this normalization expressed weld pitch in terms of travel distance per revolution per feature, possibly analogous to the "chip load" calculation that is common in machining literature [31], although this form did not yield significant insight into process.

Figure 1 demonstrates the utility of analyzing the current Data Set procedures in terms of surface velocity and volumetric flowrate. What appears to be a high travel speed, on the left of the figure, is viewed much differently in terms of volumetric flowrate. Similarly, what appears to be a low spindle speed can represent a more moderate surface velocity, depending on the size of the tool. Normalizing the data in this way offers a more rational context to compare conditions from diverse welding procedures.

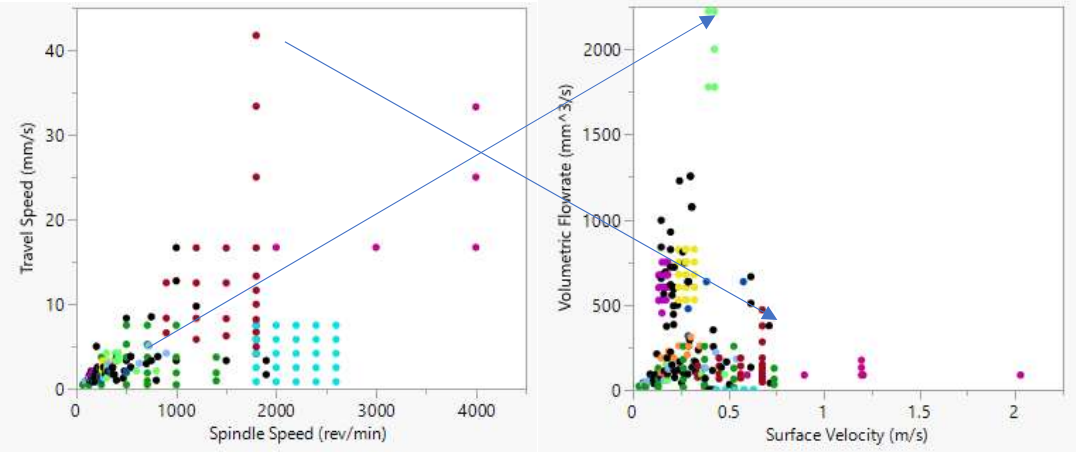

Figure 1. Map of machine parameters from the Data Set, in terms of spindle speed and travel speed (left) and in terms of surface velocity and volumetric flowrate (right).

Flow Stress

Much like the component forces and measured temperature at the tool/workpiece interface, the spindle torque reflects conditions present during welding in real time. However, taken in

its most basic form, the significance of the torque produced in a particular weld is difficult to appreciate. It is by using the torque and the welding tool geometry to calculate average flow stress that it becomes possible to grasp meaningful trends in the data.

Following the detailed analysis by Schmidt [15], a control surface that mirrors the general profile of the welding tool, just outside of the threads and other features of the tool, experiences plastic deformation at practically all points. The contact shear stress on this surface is therefore equal to the shear flow stress in the workpiece. To calculate normal flow stress, the average shear yield stress is first calculated by dividing the measured spindle torque by the surface integral of the radius,

$$\tau_{yield} = \frac{T}{\int_S r\, dA} = \frac{T}{G} \tag{5}$$

where T is the spindle torque and S is the total surface of the tool, including the shoulder, the probe sides and the probe end. For a flat or tapered shoulder and a frustum or cylindrical probe,

$$\tau_{yield} = \frac{T}{\frac{2\pi}{3}\left[\frac{S^3 - {P_r}^3}{\cos\alpha} + \frac{t((P_R + P_T)^2 - P_R P_T)}{\cos\beta} + {P_T}^3\right]} \tag{6}$$

The normal flow stress is calculated from the shear flow stress using the von Mises yield criterion,

$$\sigma_{yield} = \tau_{yield}\sqrt{3} \text{ (units: force per unit area)} \tag{7}$$

It should be noted that this calculation simply reflects an average distribution of the torque over the surfaces of the welding tool, as if the distribution was uniform. It is certain that this does not reflect reality. It is known, for example, that there are parts of the welding tool that are not in contact with the workpiece at all, based on experimental evidence [32-34]. Further, it is likely that the local flow stress and local temperature at a given point is dependent on the local surface velocity, so it should be clear that the average flow stress is not representative of local conditions at a point on the tool surface. For the purposes of this study, it does not appear necessary to have such a detailed understanding of local conditions, but calculation of the average flow stress is useful to accurately interpret some results.

Shoulder Pressure and Lateral Probe Pressure

These derived quantities are simply a way to normalize the plunge and in-plane forces with respect to tool geometry. Shoulder pressure is calculated as,

$$\text{SP} = \frac{F_{plunge}}{\pi S^2} \text{ (units: force per unit area)} \tag{8}$$

The lateral probe pressure, for a frustum or cylindrical probe, is calculated as,

$$\text{LP} = \frac{\sqrt{({F_{longitudinal}}^2 + {F_{transverse}}^2)}}{t*(P_r + P_t)/2}, \text{ (units: force per unit area)} \tag{9}$$

Heat Flux

The heat flux represents the power output per unit tool area and is calculated from the shear flow stress (Eqn. (5)) and the average surface velocity, from Eqn. (4), as:

$$\phi_q = \tau_{yield} \times \omega\bar{r} \text{ (units: power per unit area)} \quad (10)$$

Energy Density

Early research in FSW attempted to normalize heat input based on the total power output and the travel speed, yielding calculation of "specific energy" [30]. However, this formulation did not account for differences possible with respect to workpiece thickness. To improve the expression of the energy put into the workpiece, in terms of volume of processed material, the energy density can be calculated as shown below, with weld pitch calculated as the travel speed divided by the spindle speed.

$$\rho_{E1} = \frac{\phi_q \times (total\ tool\ area)}{FR} = \frac{2\pi T}{weld\ pitch \times (lateral\ probe\ area)} \text{ (units: energy per unit volume)} \quad (11)$$

There is a second possible expression of energy density that is based on the total tool area, shown below, although it remains to be seen if one expression is superior to the other in terms of data set analysis.

$$\rho_{E2} = \frac{\phi_q}{travel\ speed} = \frac{2\pi T}{weld\ pitch \times (total\ tool\ area)} \text{ (units: energy per unit volume)} \quad (12)$$

Data Set Analysis

Data was collected from published and unpublished sources for inclusion in a publicly available Data Set [1]. This data set has been greatly expanded from the original release by expanding the number of data fields to include greater detail in procedure definition, in recording outcomes and in derived quantities. The data set is no longer restricted to welds of good quality, and much of the data set expansion is related to recording various measures of weld quality. The data set is also no longer restricted to aluminum alloys, with the hope that many more procedures can be recorded for other metals. A Data Set Topics document has been added to the download, to document requirements for each data field and to include documentation of all the equations used in the Derived Quantities section of the Data Set.

The data from the Data Set was analyzed with respect to flow stress as a function of surface velocity, excluding procedures that either had no quality information or were reported to have some quality "demerit", as defined in the Data Set Topics, shown in Figure 2. It is notable that there are relatively few procedures that report flow stress values below about 20 MPa and with surface velocity values below about 0.1 m/s. Considering that only procedures that were reported to have good quality were included, it was speculated that welds below 20 MPa and below 0.1 m/s surface velocity possibly tended to have defects.

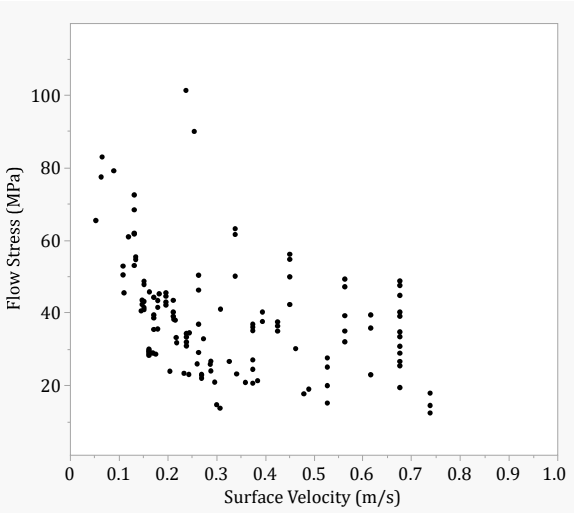

Figure 2. Flow stress vs. surface velocity, FSW Data Set [1].

Analysis of the Data Set with respect to flow stress as a function of inverse surface velocity and volumetric flowrate showed that the data for individual cohorts of procedures tended to form linear response surface planes. Figure 3 graphically summarizes the results of multiple regression analyses from each of the major cohorts in the Data Set, with key statistics listed in Table 2. In the figure, the borders represent the approximate limits of the data reported for each cohort.

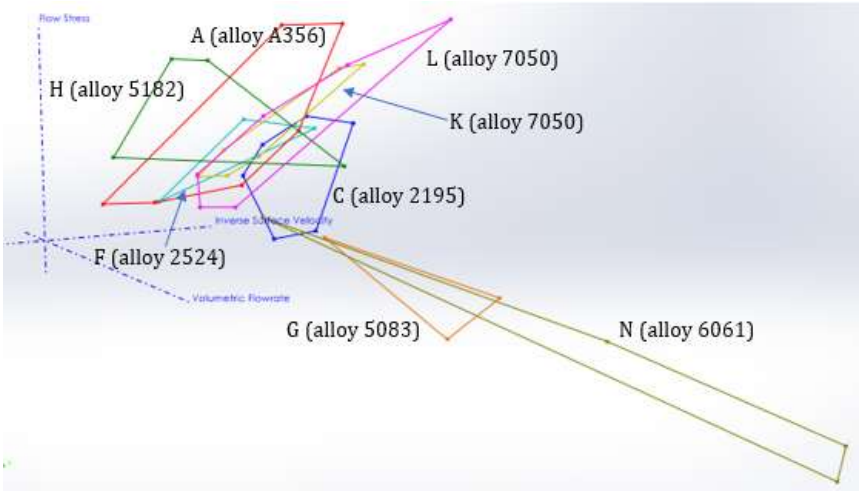

Figure 3. Flow stress response surface planes by Data Set cohort.

Table 2. Summary of multiple regression analysis of flow stress response with respect to inverse surface velocity and volumetric flowrate by Data Set cohort.

Cohort (Alloy)	Inverse Surface Velocity Coefficient	Volumetric Flowrate Coefficient	Intercept	R^2	Standard Error
	(MPa/(m/s))	(MPa/(mm^3/s))	(MPa)		(MPa)
A (A356)	8.072	0.077	-0.82	0.97	3.47
C (2195)	7.887	0.047	-17.72	0.94	2.10
F (2524)	6.307	0.051	-0.88	0.98	1.80
G (5083)	6.566	0.014	-6.07	0.95	1.12
H (5182)	19.996	0.066	-4.77	0.86	4.48
K (7050)	4.920	0.080	1.28	0.94	2.78
L (7050)	4.007	0.015	11.34	0.88	4.50
N (6061)	10.500	-0.012	-5.95	0.93	1.48

Welding Experiments

Unit-area analysis was applied to a series of welds made in nominally 25-mm and 50-mm 7050-T6 aluminum plates. Typical test plates measured 150mm by 1,200mm. All welds made were full penetration, bead-on-plate. The welding tool for the 25-mm welds had a 35.6-mm shoulder diameter that was flat and had three spiraled scrolls. The probes were frustum-shaped with threads with a 1.81-mm/thread pitch and had 5 flats, with a root diameter of 21mm and a tip diameter of 12.7mm. The two-piece tools had the probe length adjusted to about 0.5mm less than the minimum plate thickness for each weld. The tools for the 50-mm welds had a flat, scrolled shoulder with a diameter of 47mm. The probes were frustum-shaped with a 1.81-mm thread pitch and 5 flats, with a root diameter of 24mm and a tip diameter of 11.8mm, similarly adjusted for each weld with a length that was 0.5mm less than the minimum plate thickness. All welds were made with 0° tool tilt. The welding system used was CTC's FSW-H25K-5AX system, manufactured in 2000 by Mid-Columbia Engineering, shown in Figure 4.

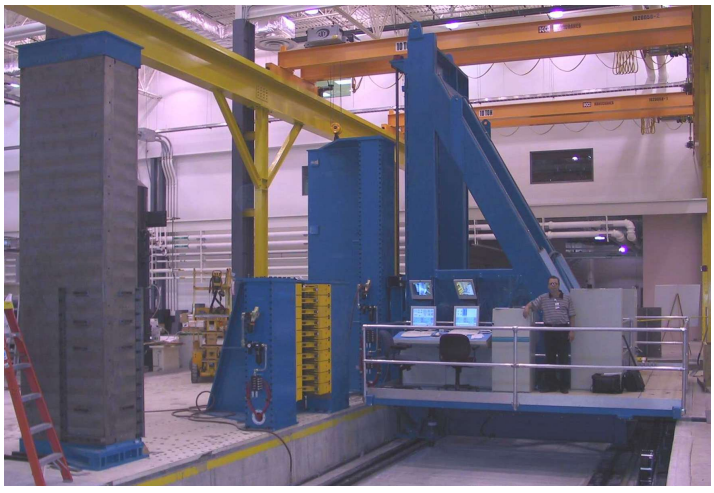

Figure 4. CTC's large FSW system.

A series of welds was made to collect force and torque data as a function of spindle speed and travel speed. Welds were made in load control, attempting to maintain a constant plunge force with all speed/feed settings. However, some adjustments were necessary due

to the broad range of settings explored. Duplicate welds were made in position control using a laser displacement sensor to reference the plate surface. To maximize the number of conditions that could be evaluated, each weld had multiple segments of different machine settings. A total of 49 unique speed/feed pairs were run in both load and position control, with selected replicates.

Each weld was inspected using phased-array ultrasonic testing (PAUT), radiographic testing (RT), macro examination and tensile testing. Each weld also had samples of the excess flash produced removed and weighed, permitting reporting of the weight of flash per unit length of weld for each weld segment. The data from each weld was analyzed to extract average force and torque values for each segment. To do this, segments of stable inputs and outputs for each segment were selected and averaged. Derived quantities were calculated from each segment of data, including surface velocity, volumetric flowrate, flow stress, heat flux and energy density.

Selections from the full scope of testing and analysis are presented here to illustrate the unit-area analysis results. Figure 5 shows flow stress, lateral probe pressure, shoulder pressure and total flash measurements for welds made at 1.27 mm/s travel speed and various spindle speeds ranging from 90 rev/min to 310 rev/min. These welds were made in load control with a shoulder pressure of about 51 MPa. The flash observed was zero below about 0.15 m/s surface velocity but above that value increased with increasing surface velocity. Below 0.15 m/s surface velocity, the flow stress and the lateral probe pressure were nearly equal and increased with decreasing surface velocity. These values diverged above 0.15 m/s surface velocity, with the flow stress continuing its previous trend while the lateral probe pressure increased continuously.

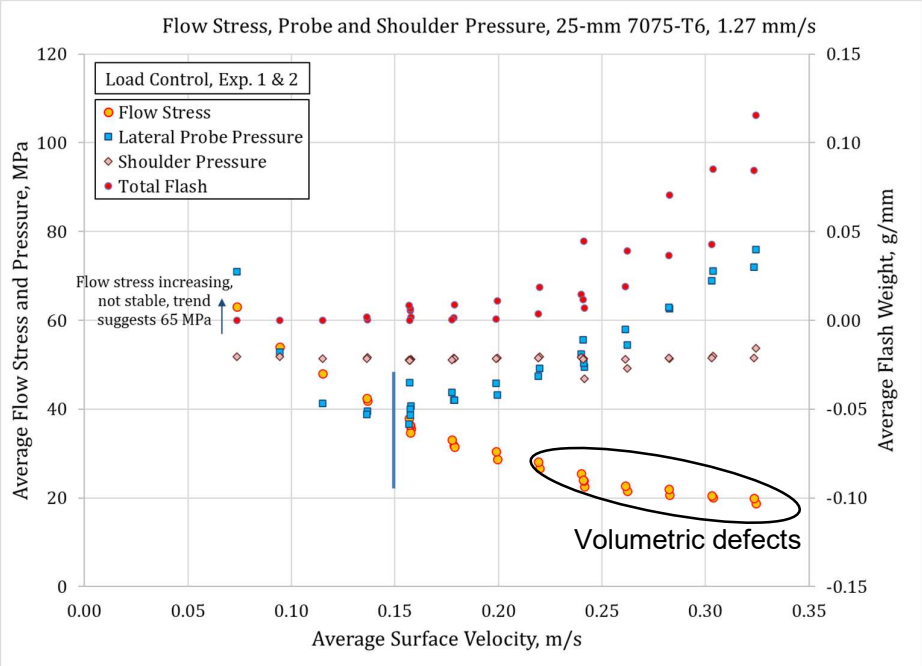

Figure 5. Flow stress, lateral probe pressure and total flash as a function of average surface velocity, 1.27 mm/s travel speed, 25-mm 7075-T6 aluminum, averages from multiple weld segments.

Study of the data from these experiments suggested that heat flux was generally linear with respect to travel speed. Using this as an assumption, it can be shown that if heat flux is linear with respect to travel speed, then flow stress must be linear with respect to the inverse

of the surface velocity. When the flow stress data from Figure 5 is plotted against the inverse surface velocity, the linear trend emerges, as shown in Figure 6. The slope with respect to inverse surface velocity agrees favorably with results from Cohorts K and L in Table 2, which are from welds in 6.4-mm 7050 aluminum.

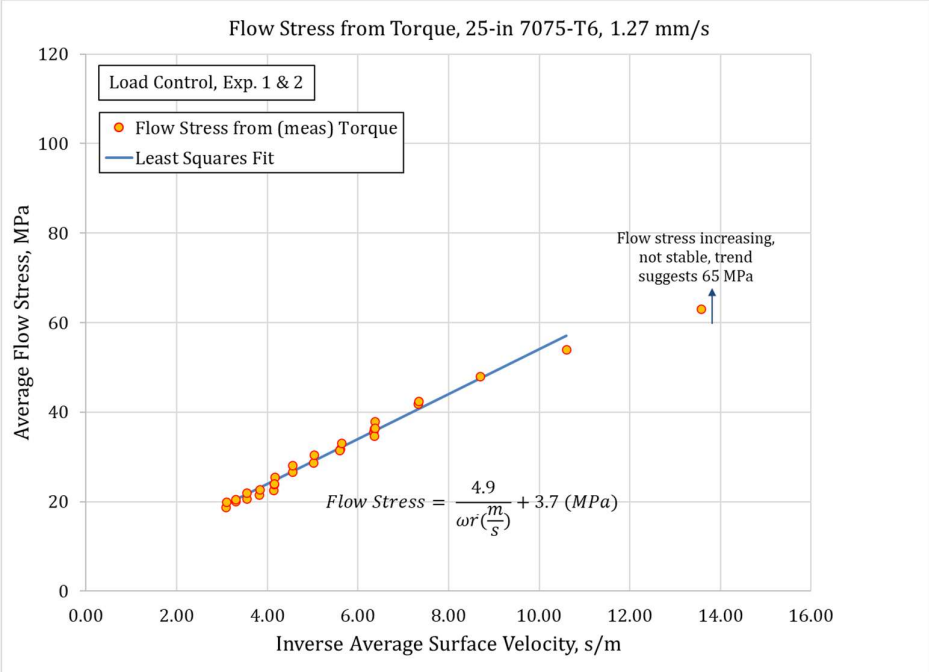

Figure 6. Flow stress as a function of inverse surface velocity, 25-mm 7075-T6 aluminum at 1.27 mm/s travel speed.

Multiple regression analysis was run on the 25-mm welds using inverse surface velocity and volumetric flowrate as independent variables. The regression results yielded the prediction expression below with a root mean squared error of 1.2 MPa and a R^2 value of 0.998, in good agreement with other results for this alloy in Table 2. The flow stress response surface is presented graphically in Figure 7.

$$\sigma_{yield} = \frac{4.85}{SV} + 0.021 \times FR - 5.76 \tag{13}$$

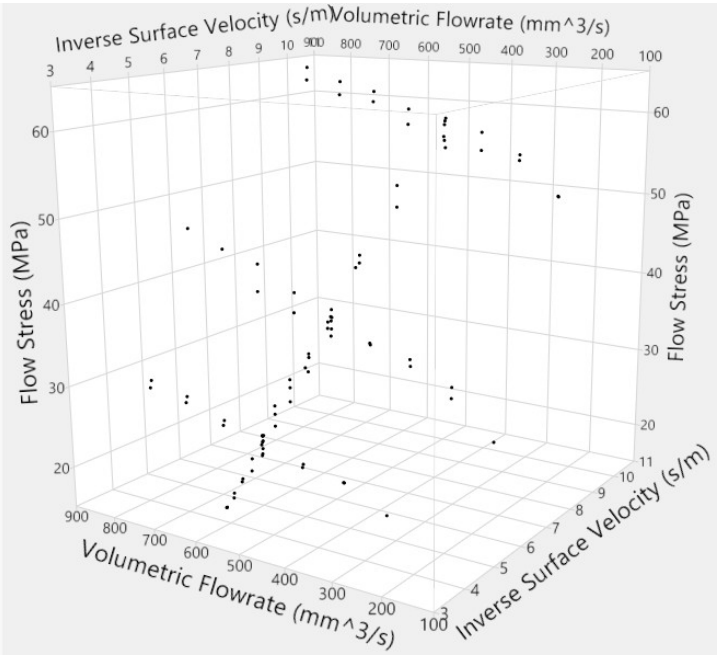

Figure 7. Scatter plot of flow stress as a function of volumetric flowrate and inverse surface velocity, 25mm 7075-T6 FSW.

It was noted during analysis of the results that there seemed to be a correspondence between welds with low flow stress and volumetric defects, detected by visual inspection, PAUT, RT and macro-section examination, as indicated in Figure 5. To further test this, a flow stress defect correlation experiment was made with four levels of flow stress using three different speed/feed combinations for each. The expression in Eqn. (13) was used to determine the machine settings that would yield the desired flow stress levels. Similar welds were made in 25-mm and 50-mm 7075-T6 plates. At the time of this writing, only visual inspection for surface tearing and excess flash were available to report. Surface tearing is a volumetric defect that is visible at the surface, an example of which is shown in the macro-section shown in Figure 8. This defect has been reported elsewhere to coincide with excessive spindle speed [35] but is seen here in the context of unit-area analysis to coincide with low flow stress.

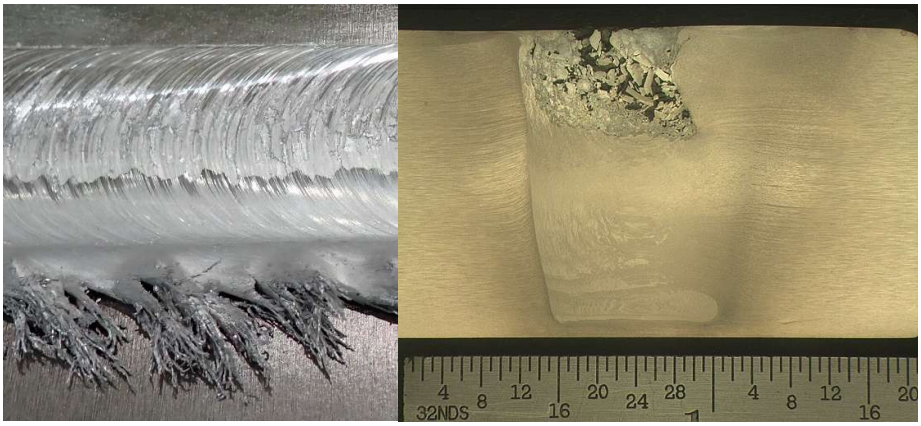

Figure 8. Typical surface-tearing observation, crown surface (left) and macro section (right), 25mm 7075-T6, 20.1 MPa average flow stress.

A summary of the results from the flow stress defect correlation experiment is presented in Table 3. Surface tearing was observed when the flow stress was at or below 22.0 MPa,

except in one case. Surface tearing was always accompanied by excess flash, although some weld segments had excess flash without surface tearing.

Table 3. Summary of flow stress defect correlation experiment, 25 and 50-mm 7075-T6.

Nominal Thickness (mm)	Flow Stress (MPa)	Surface Tearing?	Flash?
25	25.8	no	no
25	25.8	no	no
25	25.5	no	no
50	24.8	no	yes
25	24.1	no	no
25	23.8	no	no
25	23.6	no	no
50	23.3	no	no
50	22.9	no	yes
25	22.9	no	no
25	22.7	no	no
50	22.4	no	yes
50	22.2	no	no
25	22.0	yes	yes
50	21.7	yes	yes
25	20.9	yes	yes
25	20.4	yes	yes
25	20.3	yes	yes
50	18.9	no	yes
50	17.9	yes	yes
50	17.9	yes	yes
50	17.8	yes	yes
50	17.6	yes	yes
50	17.5	yes	yes

The production of excess flash was also examined. The flash observations from 116 individual 25-mm 7075-T6 weld segments were analyzed in JMP statistical analysis software by building decision tree models based on various independent variables. In this preliminary study, the most predictive data features analyzed were the difference between the shoulder pressure and the flow stress, SP-FS, referred to here as excess shoulder pressure, and the energy density, ρ_{E2} (also referred to as ED in the figure below). Based on this analysis, shown graphically in Figure 9 and tabulated in Table 4, the excess shoulder pressure and energy density are reasonable predictors of flash formation, although a larger data set is needed.

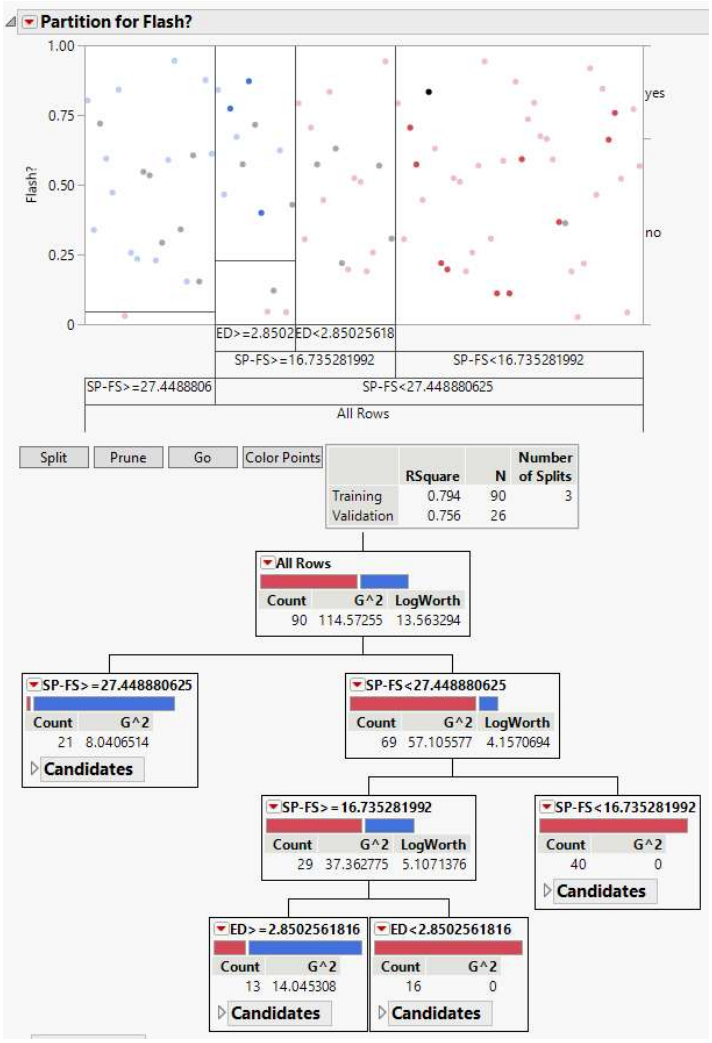

Figure 9. Decision tree analysis of shoulder pressure minus flow stress (SP-FS) and energy density (ED), 116 weld segments in 25-mm 7075-T6.

Table 4. Summary of decision tree analysis, flash formation in 25-mm 7075-T6 FSW.

SP-FS Conditions	*ED Conditions*	*Probability of Flash*
$(SP-FS) < 16.74\ MPa$		*0.76%*
$(SP-FS) \geq 16.74\ MPa$ *and* $(SP-FS) < 27.45\ MPa$	$ED < 2.85\ J/mm^3$	*1.87%*
	$ED \geq 2.85\ J/mm^3$	*73.7%*
SP-FS > 27.48		*92.4%*

The correlation between flow stress and weld quality was tested in a series of bead-on-plate welds that had variable geometry. Each panel was nominally 150mm by 1,200mm by 25mm thick. The first half of each plate was full width, providing a section of weld where conditions could be stabilized. The second half of each plate had two regions with the width reduced to 150mm, 127mm, 102mm or 76mm. Preliminary testing showed that these reduced-width sections would exhibit reduced flow stress, possibly generating surface-tearing defects if attempted with constant, "normal" machine settings. Half of the panels were welded by manually modulating the spindle speed in steps to hold a constant spindle torque (constant flow stress). Half were welded by modulating the travel speed. In the most severe cases,

with 76-mm width, both spindle speed and travel speed were modulated to hold constant torque.

Figure 10 shows plates with a 75-mm wide reduced width section that were welded in axial load control with and without flow stress control. In the weld on the left in the figure, the machine operators were instructed to navigate the weld by adjusting the plunge force to maintain uniform shoulder contact as the weld boundary conditions changed. Although they were successful in maintaining full shoulder contact with minimal flash, the surface-tearing defect commonly seen in welds with low flow stress appeared in each of the reduced-width sections. In the weld shown on the right in the figure, the flow stress was maintained at a constant 31 MPa by observing the spindle torque that was displayed in real time and adjusting both the travel speed and spindle speed to hold that torque setting. A constant shoulder pressure of about 45 MPa was maintained throughout. No defects were observed, although additional non-destructive and destructive testing is underway at this time. A similar weld, made in a panel with 100-mm width under flow stress control, exhibited no volumetric defects in the macro-section, shown in Figure 11.

Figure 10. 75-mm reduced width section without flow stress control (left) and with flow stress control (right) at a flow stress of about 31 MPa, 25-mm 7075-T6 aluminum plate.

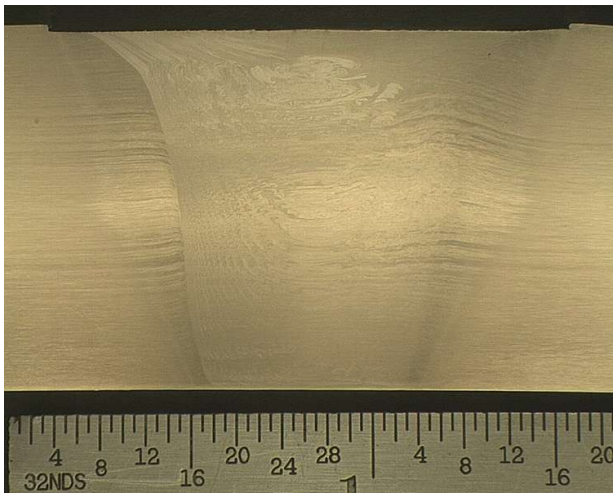

Figure 11. Macro section, 25-mm 7075-T6 at 100mm width, 31.4 MPa flow stress.

Discussion

Welds were made with different flow stress values in 25-mm and 50-mm 7075, which identified a flow stress threshold below which defects were observed. This threshold was simply based on post-weld visual inspection of surface-breaking defects. It is expected that a somewhat higher quality threshold will be indicated once full post-weld testing is completed. Future research may identify similar thresholds for other alloys, which will be most useful for broad application of flow stress control in industry and research.

There are limitations to the use of flow stress for control applications. For welding procedures that require tilting the welding tool relative to the workpiece, there is often incomplete contact between the shoulder and the workpiece. The current equations for calculating flow stress assume contact over the entire shoulder surface, so without some additional parameter representing the percentage of shoulder area in contact with the workpiece, the calculated flow stress will appear lower than actuality. This error will likely not preclude the use of flow stress control, since such an error in control will result in actual conditions that are further from producing “hot” defects.

Another limitation is related to excess flash. If excess flash is rubbing against the side of the welding tool and is sufficiently heavy, perhaps due to severe mismatch in the joint, the calculated flow stress will appear higher than actuality. This error would cause the controller to produce conditions that are closer to producing defects. Based on this, it may be necessary to restrict the allowable joint mismatch to safely use flow stress control in a production environment.

This work demonstrated that flow stress can be used as an indicator of weld quality, particularly for cases of low flow stress. However, a particular value of flow stress does not necessarily guarantee a sound weld. It is certainly possible to induce defects in a weld if, for example, a very low plunge force is used. Inadequate containment of the weld zone by forcible contact between the shoulder and the workpiece is still required, regardless of the observed spindle torque and calculated flow stress. The present work suggests maintaining a shoulder pressure that is some amount greater than the flow stress, although additional testing is required to fully establish the utility of this approach. Another way of producing defects, excessive joint gap, will produce volumetric defects regardless of the flow stress.

This work has not yet explored the production of volumetric defects associated with “cold” welding conditions that are characterized by high flow stress, generally from the low range of

surface velocity identified in Figure 2. Welds were made at high flow stress in this study and characteristic defects were observed, but the results have not yet been thoroughly evaluated or confirmed.

Closed-loop control of welding tool temperature has been developed and shown to be capable of tightly controlling the conditions of welding in FSW, even in the case of variable boundary conditions [18-26]. The relationship between peak temperature and torque is well described in the literature and torque is used in some of the temperature control methods to modulate the temperature. However, from the work described here it seems to be possible to simply control torque as a means of maintaining constant welding conditions without the need to "close the loop" on temperature. Flow stress is used here instead of torque simply to normalize the value with respect to tool geometry, although in practice it is the torque that is being controlled. The agreement between 25mm and 50mm 7075 with respect to a flow stress-based quality threshold seen here does suggest a possible universality, at least within alloy systems. Additional work is required to test the universality of flow stress with respect to tool geometry, workpiece thickness and alloy.

Conclusions

Unit-area analysis was developed as a means of analyzing a diverse collection of welding procedures, published in the form of a publicly accessible Data Set [1]. This analysis provides more meaningful data features as inputs to machine learning research. Welding conditions with low average flow stress were identified as possibly leading to welding defects, both in the Data Set and in welding experiments in 25-mm 7075 aluminum. This was tested in welds made with different flow stress levels in 25-mm and 50-mm 7075 plates and a flow stress threshold of 22 MPa was identified based on visual inspections, although it is expected that a somewhat higher threshold will emerge as destructive testing is completed. Welds in variable-geometry plates were made with and without flow stress control by manually adjusting spindle speed and/or travel speed to hold constant torque. This approach successfully produced welds with no surface defects, and destructive testing is currently underway. These preliminary results suggest that flow stress control may be a viable process control method, with some noted limitations.

Acknowledgements

This research was sponsored by the Army Research Laboratory and was accomplished under Cooperative Agreement Number W911NF-23-2-0099. The views and conclusions contained in this document are those of the authors and should not be interpreted as representing the official policies, either expressed or implied, of the Army Research Laboratory or the U.S. Government. The U.S. Government is authorized to reproduce and distribute reprints for Government purposes notwithstanding any copyright notation herein. ARL, as the Federal awarding agency, reserves a royalty free, nonexclusive and irrevocable right to reproduce, publish, or otherwise use this data for Federal purposes, and to authorize others to do so in accordance with 2 CFR 200.315(b).

References

1. https://www.ctc.com/friction-stir-welding.aspx
2. Colligan, K., "Analysis of data from friction stir welds in aluminum," International Symposium on Friction Stir Welding and Processing, The Welding Institute, Cambridge, UK, 28-30 September 2022, Luneburg, Germany.
3. Colligan, K., "Analysis of torque data from friction stir welds in aluminum alloys," Friction Stir Welding and Processing IX, TMS (the Minerals, Metals and Materials Society), pp. 75-85, 2022.

4. Feng, Z., Gould, J.E. and Lienert, T.J., “A heat flow model for friction stir welding of aluminum alloys,” Hot Deformation of Aluminum Alloys II, TMS, 1998.
5. Russell, M.J. and Shercliff, H.R., “Analytical modelling of friction stir welding,” Proc. INALCO ’98: 7th Int’l. Conf.: Joints in Aluminum, Vol 2, pp.185-217, Cambridge, UK, 16 April, 1998.
6. Frigaard, O., Grong, O. and Midling, O.T., “Modelling of heat flow phenomena in friction stir welding of aluminum alloys,” Proc. INALCO ’98: 7th Int’l. Conf.: Joints in Aluminum, Vol 2, pp.185-217, Cambridge, UK, 16 April, 1998.
7. McClure, J.C., Tang, W., Murr, L.E., Guo, X., Feng, Z. and Gould, J.E., “Thermal model in friction stir welding,” 5th Int’l. Trends in Welding Research Conference Proceedings, 1-5 June, 1998, Pine Mountain, GA, ASM Int’l, pp. 590-596, 1998.
8. Russell, M.J. and Shercliff, H.R., “Analytical modelling of microstructure development in friction stir welding,” 1st Int’l Symposium on Friction Stir Welding, The Welding Institute, Cambridge, UK 14-16 June, 1999, Rockwell Science Center, Thousand Oaks, CA, USA.
9. Chao, Y.J. and Qi, X., “Heat transfer and thermo-mechanical analysis of friction stir joining of AA6061-T6 plates,” 1st Int’l Symposium on Friction Stir Welding, The Welding Institute, Cambridge, UK 14-16 June, 1999, Rockwell Science Center, Thousand Oaks, CA, USA.
10. Colegrove, P., “3 dimensional flow and thermal modelling of the friction stir welding process,” 2nd International Symposium on Friction Stir Welding, The Welding Institute, Cambridge, UK, 28-28 June 2000, Gothenburg, Sweden.
11. Xu, S., Deng, X., Reynolds, A.P. and Seidel, T.U., “Finite element simulation of material flow in friction stir welding,” Sci. Tech. Weld. and Join., 2001, Vol. 6, No. 3, pp. 191-193.
12. Song, M., Kovacevic, R., Ouyang, J., and Valant, M., “A detailed three-dimensional transient heat transfer model for friction stir welding,” 6th Int’l. Trends in Welding Research Conference Proceedings, 15-19 April, 2002, Pine Mountain, GA, ASM Int’l., pp. 247-252, 2003.
13. Khandkar, M.Z.H., Khan, J.A. and Reynolds, A.P., “Input torque based thermal model of friction stir welding,” 6th Int’l. Trends in Welding Research Conference Proceedings, 15-19 April, 2002, Pine Mountain, GA, ASM Int’l., pp. 218-223, 2003.
14. Khandkar, M.Z.H., Khan, J.A. and Reynolds, A.P., “Prediction of temperature distribution and thermal history during friction stir welding: input torque based model,” Science and Technology of Welding and Joining, 2003, Vol. 8, No. 3, pp. 165-174.
15. Schmidt, H., Hattel, J. and Wert, J., “An analytic model for the heat generation in friction stir welding,” Modelling and Simulation in Materials Science and Engineering, 2004, Vol. 12, pp. 143-157.
16. Schmidt, H. and Hattel, J., “A local model for the thermomechanical conditions in friction stir welding,” Modelling Simul. Mater. Sci. Eng., 13 (2005) 77-93.
17. Long, T., Tang, W. and Reynolds, A.P., “Process response parameter relationships in aluminum alloy friction stir welds,” Sci. & Tech. of Weld. And Join., 2007, vol. 12, no. 4, 311-317.
18. Madigan, R.B., Shubert, B.J., Mao, Y. Butte, M.T. and Lienert, T.J., “Control of normal tool stress during friction stir welding,” FABTECH Int’l. & AWS Welding Show Conference Talk, 2007.
19. Zhao, X., Kalya, P., Landers, R.G., and Krishnamurthy, K., “Path force control for friction stir welding processes,” Proc. ASME Dynamic Systems and Control Conference, October 20-22, 2008, Ann Arbor, MI.

20. Cederqvist, L., Bolsmjo, G. and Sorensen, C.D., “Adaptive control of novel welding process to seal canisters containing Sweden’s nuclear waste using PID algorithms,” Int’l. Conf. on Flex. Auto. And Intelligent Mfg., FAIM, Skovde, Sweden, 2008.
21. Fehrenbacher, A., Pfefferkorn, F.E., Zinn, M.R., Ferrier, N.J. and Duffie, N.A., “Closed-loop control of temperature in friction stir welding,” 7th Int’l. Sym. On Friction Stir Welding, The Welding Institute, Cambridge, UK 20-22 May, 2008, Awaji Island, Japan.
22. Fehrenbacher, A., Duffie, N.A., Ferrier, N.J., Zinn, M.R. and Pfefferkorn, F.E., “Temperature measurement and closed-loop control in friction stir welding,” 8th Int’. Symp. On Friction Stir Welding, The Welding Institute, Cambridge, UK 18-20 May 2010, Timmendorfer Strand, Germany.
23. Mayfield, D.W. and Sorensen, C.D., “An improved temperature control algorithm for friction stir processing,” 8th Int’. Symp. On Friction Stir Welding, The Welding Institute, Cambridge, UK 18-20 May 2010, Timmendorfer Strand, Germany.
24. Cederqvist, L., Reynolds, A.P., Sorensen, C.D. and Garpinger, O., “Reliable FSW of copper canisters using improved process and regulator controlling power input and tool temperature,” 8th Int’. Symp. On Friction Stir Welding, 18-20 May 2010, Timmendorfer Strand, Germany.
25. Ross, K., “Investigation and implementation of a robust temperature control algorithm for friction stir welding,” MS Thesis, Department of Mechanical Engineering, Brigham Young University, April 2012.
26. Sigl, M.E., Bachmann, A., Mair, T. and Zaeh, M.F., “Torque-based temperature control in friction stir welding by using a digital twin,” Metals, Vol. 10, 914, 8 July, 2020.
27. Longhurst, W.R., “Force control of friction stir welding,” PhD Dissertation, Vanderbilt University, Nashville, TN, 2009.
28. Longhurst, W.R., Strauss, A.M., Cook, G.E. and Fleming, P.A., “Torque control of friction stir welding for manufacturing and automation,” Int. J. Adv. Manuf. Technol., 51(9): 905-913, 2010.
29. Andrade, D.G., Leitao, C., Dialami, N., Chiumenti, M. and Rodrigues, D.M., “Modelling torque and temperature in friction stir welding of aluminum,” Int. Journal of Mechanical Sciences, Vol. 182, 16 May, 2020.
30. Reynolds, A.P. and Tang, W., “Alloy, tool geometry and process parameter effects on friction stir weld energies and resultant FSW joint properties,” Friction Stir Welding and Processing, TMS, 4-8 November 2001, Indianapolis, IN, pp. 15-23.
31. Colligan, K., Xu, J. and Pickens, J.R., “Welding tool and process parameter effects in friction stir welding of aluminum alloys,” Friction Stir Welding and Processing II, TMS, March 2-6, 2003, San Diego, CA, pp. 181-190.
32. Colligan, K., “Dynamic material deformation during friction stir welding of aluminum,” 1st Int’l Symposium on Friction Stir Welding, The Welding Institute, Cambridge, UK 14-16 June, 1999, Rockwell Science Center, Thousand Oaks, CA, USA.
33. Colligan, K., “Material flow behavior during friction stir welding of aluminum,” Welding Journal, American Welding Society, Vol. 78(7): 229s-237s.
34. Colligan, K. and Chopra, S.K., “Examination of material flow in thick section friction stir welding of aluminum using a stop-action technique,” 5th Int’l. Symp. on Friction Stir Welding, The Welding Institute, Cambridge, UK, 14-16 Sept. 2004, Metz, France.
35. Leitao, C., Louro, R. and Rodrigues, D.M., “Using torque sensitivity analysis in accessing friction stir welding/processing conditions,” J. Mater. Proc. Tech., 212 (2012), pp. 2051-2057.